Control of interferences in an Autler-Townes doublet: Symmetry of control parameters

M. Wollenhaupt, A. Assion, O. Bazhan, Ch. Horn, D. Liese, Ch. Sarpe-Tudoran, M. Winter, and T. Baumert
Fachbereich Physik, Universität Kassel, Heinrich-Plett-Strasse 40, D-34132 Kassel, Germany
(Received 26 November 2002; published 18 July 2003)

Coherent control beyond population control and spectral interferences is demonstrated on the interferences and intensity of the two Autler-Townes (AT) components in the photoelectron spectrum of *K* atoms, using a sequence of two intense time-delayed femtosecond laser pulses. Photoelectron spectra were taken at various delay times between the two laser pulses and at different laser intensities at a fixed delay time. With respect to the interferences in the AT doublet the role of time delay and laser intensity is interchangeable for $(n+0.5)\pi$ excitation. Strong laser fields or the optical phase of the delayed laser pulse allow the quantum mechanical phase of an atomic state to be manipulated in a symmetrical fashion. The observations are discussed in terms of a two-level model coupled to the continuum. For suitable combinations of the laser intensity of the first pulse and the time delay, the second laser pulse leaves the excited state population unchanged.

DOI: 10.1103/PhysRevA.68.015401 PACS number(s): 32.80.Qk, 32.80.Rm, 42.50.Md

Real time observation and control of quantum phenomena in atoms and molecules with the help of advanced laser techniques is an exciting fast growing research area challenging likewise theorists and experimentalists [1]. Many different schemes for quantum control have been demonstrated proving that the operating principle of control is based on various sources of quantum mechanical interference. In particular, the use of pulse sequences has proven a strong tool to study interference effects in atomic and molecular systems in detail [2]. This scheme was extended to the continuum in order to demonstrate the coherence transfer from femtosecond laser pulses to ultrashort free electron wave packets [3] and wave packets of a dissociating molecule [4]. A variety of important control mechanisms are only accessible when strong laser fields are employed. Examples of coherent control by intense sequential laser pulses are coherent transients such as the photon echo and Ramsey fringes [5] as well as the STIRAP [6] and a theoretical study on fine structure wave packets [8]. In this contribution we focus on the control of the quantum mechanical phase of an atomic state in strong laser fields and investigate the symmetry of the control parameters delay time and laser intensity. A sequence of two intense laser pulses is used to excite *K* atoms in an atomic beam from the $4s$ to the $4p$ state. Simultaneously, the pulses ionize the excited atoms from the $4p$ state to the continuum via two-photon ionization (Fig. 1). Since the photoelectron spectrum is directly related to the temporal evolution of the excited state, energy resolved photoelectron spectroscopy is most suited to elucidate details of the quantum dynamics [7]. Photoelectron spectra were taken at various delay times between the two laser pulses and at different laser intensities at a fixed delay time. The paper is organized as follows. First we give a theoretical description of the physical model, then we present the experimental results and a discussion with respect to the suggested model.

For the theoretical description of the experiment an analytical model similar to the photon echo formalism [5] is adopted using the following simplifications: (1) the *K* atoms are treated as a two-level system, (2) the laser pulses are separated in time, (3) the driving field frequency ω_0 is resonant with the transition frequency ω_{ba}, (4) the rotating-wave approximation is made. Effects due to the 7 meV spin-orbit splitting of the $4p$ state take place on a 580 fs time scale and can be neglected in our experiment. For the first pulse, the Schrödinger equation yields the solution for the excited state amplitude $c_b(t)$:

$$c_b(t) = i\sin\left(\frac{\theta(t)}{2}\right)$$

with

$$\theta(t) = \int_{-\infty}^{t} \Omega(t')dt', \tag{1}$$

where $\theta(t)$ describes the time-dependent pulse area and $\hbar\Omega(t) = \mu\varepsilon(t)$ describes the instantaneous Rabi frequency with μ being the dipole moment and $\varepsilon(t)$ the electrical field envelope (Fig. 1). The initial condition for the second pulse

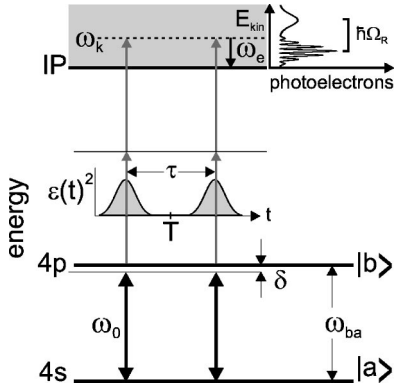

FIG. 1. Energy level diagram for excitation of *K* atoms. A sequence of two time-delayed (τ) 30 fs FWHM laser pulses with an intensity envelope $\varepsilon(t)^2$ and a carrier frequency ω_0 (corresponding to 785 nm) detuned from the resonance frequency ω_{ba} (768 nm) drives Rabi oscillations (black arrows) between the lower $4s$ ($|a\rangle$) and the upper $4p$ ($|b\rangle$) states of *K* atoms. Photoelectrons with a kinetic energy $E_{kin} = \hbar\omega_e$ from simultaneous two-photon ionization (gray arrows) of the $4p$ state to the continuum (ω_k) are measured. The observed AT doublet—split by $\hbar\Omega_R$—shows interferences.

is given by $c_b(T)=i\sin(\Theta/2)$, where $\Theta=\theta(T)$ denotes the area of the first pulse. For the second pulse the time evolution of the excited state is given by

$$c_b(t)=i\left[s\cos\left(\frac{\theta(t-\tau)}{2}\right)+e^{i\omega_0\tau}c\sin\left(\frac{\theta(t-\tau)}{2}\right)\right], \quad (2)$$

where $c=\cos(\Theta/2)$ and $s=\sin(\Theta/2)$. Since the coupling of the $4p$ state to the ionization continuum is much smaller than the coupling to the $4s$ state, the two-photon ionization can be described in the weak-field limit [9]:

$$c(\omega_e)\propto\int_{-\infty}^{\infty}e^{i(\omega_k-\omega_{4p})t'}c_b(t')E^2(t')dt', \quad (3)$$

where $E(t)$ denotes the electrical field of both pulses and $c(\omega_e)$ denotes the amplitude of a continuum state with an energy $\hbar\omega_k$ labeled according to the kinetic energy of the photoelectron $\hbar\omega_e$, and $|c(\hbar\omega_e)|^2$ describes the photoelectron spectrum. Results of the resonant calculations are presented in Fig. 2 for two different pulse areas and four delay times. Evaluation of the integral [Eq. (3)] reveals that for $\Theta=(n+0.5)\pi$ excitation the structure of the photoelectron spectrum is uniquely determined by the parameter $f=e^{i(\Theta+\omega_0\tau)}$. For $f=+1(f=-1)$, high (low) kinetic energy photoelectrons have a higher intensity and show interference fringes. For further discussions see also the caption of Fig. 2. In addition to the resonant case investigated analytically, the nonresonant case was considered by computer simulations, showing that the analytical analysis is adequate for an understanding of the dynamics. Details of the formalism will be given in a forthcoming publication. A rigorous treatment of phase control of an AT doublet in a bichromatic laser field based on numerically solving the three-dimensional Schrödinger equation is reported in Ref. [10].

The experiments were carried out in a high vacuum chamber where a beam of atomic potassium K $(4s)$ intersects perpendicularly with the femtosecond laser pulses leading to photoionization. The released photoelectrons are detected employing a magnetic bottle time-of-flight electron spectrometer with an energy resolution of 25 meV at a kinetic energy of 1 eV. The 785 nm, 30 fs full width at half maximum (FWHM) laser pulses provided by an amplified 1 kHz Ti:sapphire laser system are split into two beams using a Mach-Zehnder interferometer. The time delay of the identical laser pulses was set by the variation of the length of one arm of the interferometer and measured interferometrically with the spectral interferences simultaneously recorded by an optical spectrometer [cf. insets to Figs. 3(c), 3(d), 4(c), and 4(d)]. In the first experiment the time delay τ is varied in a range of 80–100 fs with 0.2 fs resolution at a fixed laser intensity of I_0 $(0.54\times10^{12}$ W/cm$^2)$. In the second experiment the time delay is kept fixed at 98.6 fs, whereas the energy of both beams is varied from $0.7I_0$ to $3I_0$, using a reflective variable neutral density attenuator.

At first, we discuss the results of the experiment using a variable time delay at a fixed laser intensity of I_0. Figure 3(b) shows the measured photoelectron spectra as a function of the delay time. Oscillations in the photoelectron signal at

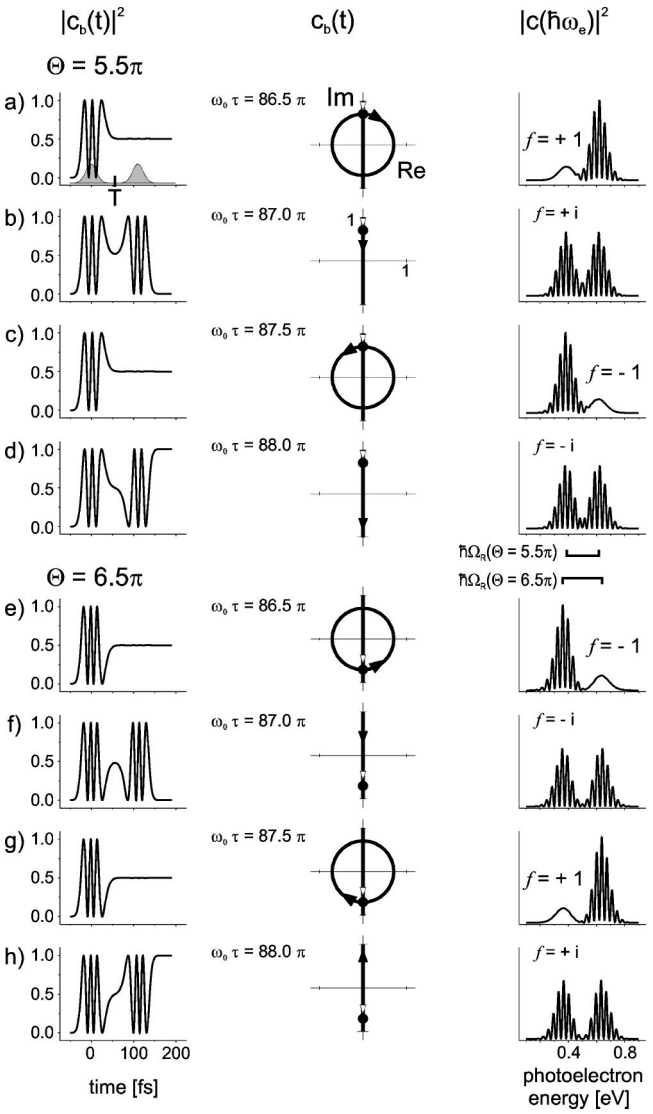

FIG. 2. Calculations for resonant two-pulse excitation-photoionization of K atoms: time dependence of the population $|c_b(t)|^2$, parametric plot of $c_b(t)$ in the complex plane, and corresponding photoelectron spectra $|c(\hbar\omega_e)|^2$ for a pulse area of $\Theta=5.5\ \pi$ (a)–(d) and $\Theta=6.5\ \pi$ (e)–(h) at four different delay times τ. Note the increase of the AT splitting $\hbar\Omega_R$ with increasing pulse area. In the upper left plot the intensity envelope $\varepsilon(t)^2$ (gray) is depicted for comparison. In the complex representation of the time evolution, $c_b(t)$ starts at the origin along the imaginary axis, the open (filled) arrows indicate the direction towards the end of the first (second) pulse, and the dot denotes the initial condition $c_b(T)$ for the second pulse. For each combination of delay time τ and pulse area Θ the characteristic parameter $f=e^{i(\Theta+\omega_0\tau)}$ is given. Note that a variation of the time delay at a fixed pulse area [cf. (a) and (c)] and a variation of the pulse area (laser intensity) at a fixed time delay [cf. (a) and (e)] lead to the same oscillations of the intensity and interference structure of the photoelectrons. Note also that for (a), (c), (e), and (g) the second intense laser pulse has no effect on the population of the $4p$ state, and the photoelectron spectrum shows fringes only in one of the AT components.

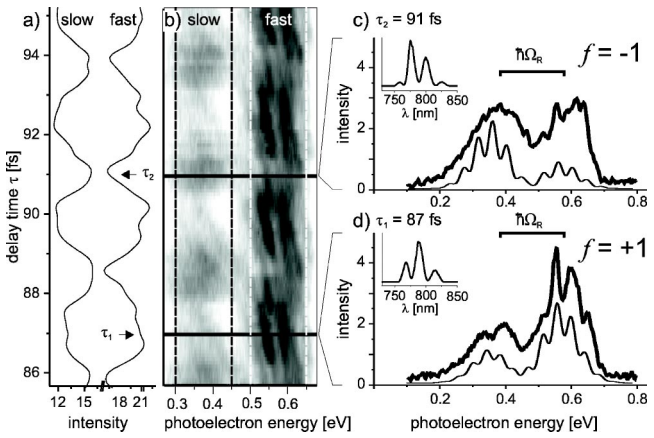

FIG. 3. Experimental photoelectron spectra (b) as a function of the delay time τ at a fixed laser intensity of I_0 (0.54×10^{12} W/cm^2). Note the slow and fast electrons being out of phase. An averaged section along the delay axis for slow (≈ 0.37 eV) and fast (≈ 0.57 eV) photoelectrons (a) highlights the π phase shift. Sections along the energy axis yield measured photoelectron spectra (bold) at $\tau_2 = 91.0$ fs (c) and $\tau_1 = 87.0$ fs (d). For labels $f = \pm 1$ see Fig. 2. $\hbar\Omega_R$ reflects the AT splitting. Simulated spectra for the respective delay times τ_1 and τ_2 convoluted with 25 meV spectrometer resolution are given for comparison. The insets to (c) and (d) show the simultaneously recorded optical spectra. Photoelectron intensities are given in arbitrary units.

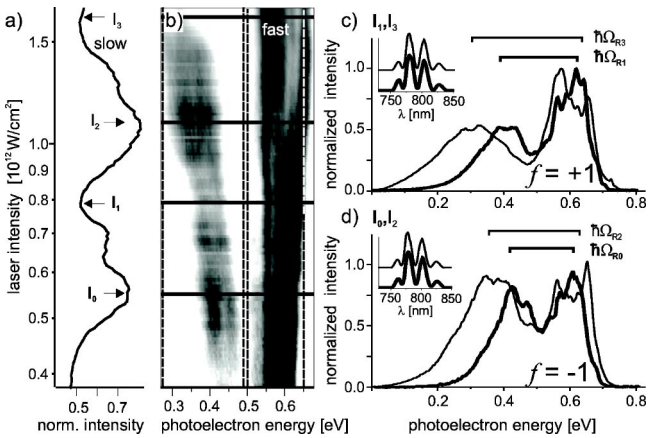

FIG. 4. Measured photoelectron spectra (b) as a function of the laser intensity at a fixed delay time of 98.6 fs. For the visualization of the out-of-phase oscillations of the two AT components with increasing laser intensity, the spectra are normalized with respect to the fast photoelectrons (≈ 0.57 eV). The averaged signal over the slow photoelectrons along the laser intensity axis (a) reveals oscillations (cf. Fig. 2). At the laser intensities of I_0 (bold), $I_2 = 2I_0$ (c), and $I_1 = 1.5I_0$ (bold), $I_3 = 3I_0$ (d), sections along the electron energy axis are shown. Although the AT splitting $\hbar\Omega_R$ monotonically increases with the laser intensity [v-shaped structure in (b)], the slow photoelectrons vary periodically [compare (c) and (d), and the oscillatory intensity variation in (b)]. Simultaneously recorded optical spectra as shown in the insets to (c) and (d) demonstrate the coherent control beyond spectral interference.

the period of the photon frequency of 2.6 fs are observed. Note that the oscillations of slow and fast photoelectrons are out of phase. Sections through the photoelectron distribution were taken along the time delay axis averaging over a range of 0.5–0.65 eV (0.3–0.45 eV) for the fast (slow) photoelectrons. The resulting time profiles shown in Fig. 3(a) highlight the π phase shift in agreement with the analytical model (Fig. 2). A comparison of measured and simulated photoelectron spectra is given in Figs. 3(c) and 3(d) for a time delay of 91.0 fs and 87.0 fs, respectively. Fast photoelectrons show the predicted fringes [Fig. 3(d)], which are not seen in the slow contributions due to the reduced spectral resolution for very slow photoelectrons. Moreover, the absolute intensity of slow photoelectrons is slightly underestimated in the experiment, since the detection efficiency for slow photoelectrons is somewhat lower. The experimental photoelectron spectra are in good agreement with the off-resonant simulations confirming the intensity oscillations of the two AT components with the time delay τ from our analytical resonant model [Fig. 2(a)–2(d) or 2(e)–2(h)]. The insets to Figs. 3(c) and 3(d) show the spectral interferences at the respective time delays.

In the second experiment the laser intensity was varied but the time delay was fixed at 98.6 fs in order to demonstrate that the control of the interferences is determined by the quantum mechanical phase, showing the symmetry of time and intensity. The optical spectrum of the pulse sequence remains unchanged for all intensities [cf. insets to Figs. 4(c) and 4(d)]. In order to compare measurements at different laser intensities, the photoelectron spectra were divided by the averaged signal over the fast electrons in a range from 0.5 to 0.65 eV, and, therefore, bring out the relative intensity of the slow photoelectrons. Photoelectron spectra normalized in this manner are displayed in Fig. 4(b) as a function of the laser intensity. A monotonic increase of the splitting of both AT components with increasing laser intensity reflected in the v-shaped structures in Fig. 4(b) is observed. The asymmetry of the splitting is due to the nonresonant excitation. In addition, the slow electron signal exhibits pronounced oscillations as the intensity is increased. A time profile of the slow photoelectron signal is obtained by suitable averaging over the low-energy part of the spectrum along the laser intensity axis. The time profile reveals an oscillatory behavior with maxima at I_0 and $I_2 = 2I_0$, and minima at $I_1 = 1.5I_0$ and $I_3 = 3I_0$. The observed periodic oscillations are in good agreement with the theoretical model shown in Fig. 2 [compare calculated photoelectron spectra with the same time delay at a different pulse area, e.g., (a) and (e)]. Normalized photoelectron spectra at the maxima (I_0, I_2) and minima (I_1, I_3) are shown in Figs. 4(d) and 4(c). The bars indicate the AT splitting, providing an independent *in situ* check for the laser intensity increasing from I_0 to I_3. However, the shape of the photoelectron spectra is periodically reproduced. Note the similarity of the photoelectron spectra for the intensity variation and for the time delay variation. In both cases an oscillatory behavior of slow and fast photoelectron intensities is observed. In particular, comparisons of the spectra at $\tau = 87.0$ fs [Fig. 3(d)] with the spectra at I_1 and I_3 [Fig. 4(c)] on the one hand (case $f = +1$) and the spectra at $\tau = 91.0$ fs [Fig. 3(c)] with the spectra at I_0 and I_2 [Fig. 4(d)] on the other hand (case $f = -1$) show

a remarkable similarity, also seen in Fig. 2 by comparison of photoelectron spectra belonging to different delay times and different pulse areas [e.g., (a) and (g) on the one hand (case $f=+1$) and (c) and (e) on the other hand (case $f=-1$)].

The observed control mechanism is discussed in terms of the population dynamics $c_b(t)$ (Fig. 2). The intensity of the first laser is high enough to cause the Rabi cycling and, therefore, AT splitting in the photoelectron spectrum. Using two identical time delayed pulses leads to fringes in the photoelectron spectrum, as discussed in Ref. [3]. The observed control of interference in the AT doublet arises if the intensity of the first pulse is chosen to yield a population of $|c_b(T)|^2=0.5$, i.e., $\Theta=(n+0.5)\pi$. According to Eq. (1) this condition may be realized by $c_b(T)=\pm i/\sqrt{2}$ [cf. (Fig. 2) $c_b=+i/\sqrt{2}$ for $\Theta=5.5$ and $c_b=-i/\sqrt{2}$ for $\Theta=6.5$]. The subsequent time evolution ($t>T$) of c_b depends on the phase $\omega_0\tau$ of the second laser pulse. In order to stress the symmetry of Θ and $\omega_0\tau$, the results are discussed using the quantity $f=\exp[i(\Theta+\omega_0\tau)]$. If $\omega_0\tau$ is a multiple integer of π and hence $f=\pm i$, the population evolves during the second laser pulse much the same way as during the first pulse, i.e., c_b stays purely imaginary and both AT components show interference fringes [(b), (d), (f), and (h) in Fig. 2]. The time evolution of the population may be symmetric with respect to T leaving the $|b\rangle$ state eventually unpopulated [(b) and (f) in Fig. 2] or asymmetric associated with a 100% population transfer [(d) and (h) in Fig. 2]. In the present experiment these cases are not distinguished. However, if the phase $\omega_0\tau$ takes half integer multiples of π, i.e., $f=\pm 1$, the experimental results are considerably different (compare photoelectron spectra labeled $f=+1$ and $f=-1$ in Fig. 2 for calculations and Figs. 3 and 4 for measurements). We encounter a surprising population evolution in which $|c_b(t)|^2$ is unchanged during the second laser pulse and only the quantum mechanical phase is altered. This results in c_b moving on a circle in the complex plane (cf. Fig. 2). Hence, during the second laser pulse the excited state acquires additional quantum mechanical phase. With regard to photoionization [cf. Eq. (3)] the additional phase may also be interpreted as a frequency shift of the ionizing field. The frequency of the second pulse may be regarded as risen or lowered leading to interference only in one of the AT sidebands. Fringes in the high (low)-energy photoelectrons are observed if c_b rotates (counter) clockwise, i.e., $f=+1$ ($f=-1$) in Figs. 2(a) and 2(g) [2(c) and 2(e)].

We demonstrate coherent control in strong fields beyond (i) population control and (ii) spectral interference, since (i) control is achieved without altering the population during the second intense laser pulse and (ii) the quantum mechanical phase is controlled without changing the spectrum of the pulse sequence. The control mechanism relies on the interplay of the quantum mechanical phase set by the intensity of the first pulse and the phase of the second pulse determined by the time delay. This phase interplay is observed as a variation of interferences and intensity in the AT doublet. In contrast to a photon echo experiment, in which the polarization is averaged over the inhomogeneous broadening *after* the pulse sequence, and the Ramsey fringes experiments, in which the upper level probability is measured *after* the pulse sequence, we use photoionization to directly follow the time evolution of the quantum mechanical amplitude of the excited state *during* the pulses. Our results show that for suitable excitation conditions the role of time delay and the laser intensity is symmetric with respect to the variation of the AT components. This equivalence is expressed by the parameter $f=\exp[i(\Theta+\omega_0\tau)]$, which uniquely describes the measurable outcome of the experiment. Since a variation of the pulse width at constant laser energy is associated with a change of the pulse area Θ and a variation of the detuning alters the phase $\omega\tau$ and the excited state population, the demonstrated control of the interference could also be accomplished by the variation of the pulse width and detuning.

The support of the Deutsche Forschungsgemeinschaft, the Fonds der Chemischen Industrie, and the NRC-Helmholtz program is gratefully acknowledged.

[1] A. Assion *et al.*, Science **282**, 919 (1998); T.C. Weinacht *et al.*, Phys. Rev. Lett. **80**, 5508 (1998); A.H. Zewail, J. Phys. Chem. A **104**, 5660 (2000); S. A. Rice and M. Zhao, *Optical Control of Molecular Dynamics*, (Wiley-Interscience, New York, 2000); H. Rabitz *et al.*, Science **288**, 824 (2000); M. Shapiro and P. Brumer, Trans. Faraday Soc. **93**, 1263 (1997).

[2] N.F. Scherer *et al.*, J. Chem. Phys. **93**, 856 (1990); M.A. Bouchene *et al.*, Eur. Phys. J. D **2**, 131 (1998).

[3] M. Wollenhaupt *et al.*, Phys. Rev. Lett. **89**, 173001 (2002).

[4] E. Skovsen *et al.*, Phys. Rev. Lett. **89**, 133004 (2002).

[5] P. Meystre and M. Sargent III, *Elements of Quantum Optics*, 3rd ed. (Springer, Berlin, 1999), Chap. 12; B.W. Shore, *The Theory of Coherent Atomic Excitation* (Wiley-Interscience, New York, 1990), Vol. 1, Chap. 3.

[6] N.V. Vitanov *et al.*, Adv. At., Mol., Opt. Phys. **46**, 55 (2001).

[7] See, for example, work on the Na_2 prototype: A. Assion *et al.*, Phys. Rev. A **54**, R4605 (1996); T. Frohnmeyer *et al.*, Chem. Phys. Lett. **312**, 447 (1999).

[8] C. Nicole *et al.*, J. Mod. Opt. **49**, 183 (2002).

[9] Ch. Meier and V. Engel, Phys. Rev. Lett. **73**, 3207 (1994).

[10] U. Lambrecht *et al.*, Phys. Rev. A **57**, R3176 (1998).